Robotica: (2021) volume 39, pp. 468–482. © The Author(s), 2020. Published by Cambridge University Press.
doi:10.1017/S026357472000051X

Design and Kinematics of a Comanipulated Robot Dedicated to Prostate Brachytherapy

Mozert Djohossou†, Aziza Ben Halima†, Antoine Valérie‡, Julien Bert†¶* and Dimitris Visvikis†¶

†*Laboratory of Medical Image Processing (LaTIM), INSERM-UMR 1101, Brest, France*
‡*Urology Department, Brest Regional University Hospital, Brest, France*

(Accepted May 28, 2020. First published online: June 22, 2020)

SUMMARY
In brachytherapy, the manual implantation of seeds is not accurate leading to side effects and limiting the use of new procedures. Robotics solutions have to be fully suitable for medical applications especially considering the operating room. This paper investigates a delta robot solution for improving the accuracy of the prostate brachytherapy procedure by proposing a compact and lightweight robot. In addition, the design was thought as a comanipulated robot for a better acceptability and human–machine interaction. The robot kinematics and singularities were determined and the theoretical capability in term of resolution and force feedback was evaluated. A prototype was built in order to experimentally measure the capability of this first prototype.

KEYWORDS: Medical robotics; Comanipulation; Prostate brachytherapy.

1. Introduction

Prostate cancer is the third leading cause of cancer deaths in the male population. Within this context, low-dose rate brachytherapy is a widely used low-risk technique for treatment of early stage cancer.[1] In this technique, radioactive seeds are inserted inside the prostate in order to treat the carcinogenic cells. These seeds are inserted under two-dimensional (2D) transrectal ultrasound (2D-TRUS) control using needles through a transperineal grid with several needle guides regularly spaced to 5 mm (called template). In order to deliver a homogeneous tumoricidal dose to the whole gland while sparing the healthy surrounding tissues and organs at risk, the number of seeds and their positions in the prostate are determined using a treatment planning system.

The current brachytherapy procedure is a long and an arduous work. Clinician has to implant 80–100 seeds within an organ which has a size of a walnut. This procedure requires practice and expertise to insert each needle in its target position using TRUS imaging. Due to the manual insertion and the poor quality of images from TRUS, seeds implantation is not accurate and never follows exactly the treatment plan. This leads to nonnegligible posttreatment side effects.[3] This issue of accuracy limits as well the possibility to study and implement new procedures. For instance, localized treatment restricted to a cancerous zone may improve the quality of life of the patient by decreasing the toxicity.[2] Such treatment may as also decrease the cost and the time of the surgery by using less seeds. However, a localized treatment requires seed placement of <4 mm accuracy,[19] which is not feasible using the current brachytherapy procedure. Robotic systems designed and developed for brachytherapy are expected to enhance the quality of care and improve the accuracy of needle

¶These authors share senior authorship
* Corresponding author. E-mail: julien.bert@univ-brest.fr

placement, and seeds delivery to ensure safety and reliability. The state of the art in assisted needle insertion for prostate brachytherapy mostly relies on several creative designs of robotic devices that have been successfully tested and validated on phantoms. The first microseeds implanting systems for brachytherapy appeared in the beginning of 1980s but they were not qualified as robotic systems.[4] In 2001, Elliot and the coauthors proposed a seed implantation system featuring automated 3D motion.[5] In 2002, Fichtinger et al. explored the use of a computer tomography guided robot containing a passive arm with seven degrees of freedom (7-DOFs).[28] After in 2004, the same group developed a device with 3-DOFs to integrate transrectal needle insertion with an ultrasound probe.[6] Later in 2007, they proposed a 4-DOF system based on the use of two 2D Cartesian motion stages arranged in parallel configuration. Clinical feasibility and performance of this system were reported in 2011.[7] In 2004, Wei et al. suggested using a commercial industrial robot to evaluate needle insertion for prostate brachytherapy.[8] Davies and his colleagues developed an XYZ robot with needle rotation.[1] Tests on the robotic demonstrator show the feasibility and performances of the system. In 2005, Okazawa et al. performed a novel handheld steerable needle device.[9] Phee et al. designed a 9-DOF stiff platform structure for percutaneous biopsy.[10] Meltsner et al. proposed a 6-DOF robotic system that enables needle inclination at a random angle with automatic positioning of radioactive seeds.[11] In 2006, Yu et al. reported a transtrectal ultrasound image guided 16-DOF prostate brachytherapy robotic system. Provisions for needle motion and force feedback had been included to improve robot control and seeds delivery. After, the same group developed in 2007 a multichannel robotic system that inserts multiple needles simultaneously in order to provide a faster needle implant and reduce tissue deformation.[26] Later in 2006, Bassan et al. proposed a new 5-DOF remote center of compliance manipulator capable of performing percutaneous needle insertion under 3D ultrasound guidance.[12] It's based on a Macro-Micro system that performs orientation, insertion and rotation of the needle and features back-derivable joints with redundant sensing. In 2008, Salcudean et al. suggested the use of a 4-DOF robot that can translate and rotate the needle in the *XY* plane.[13] This system can be mounted on a standard brachytherapy stepper when the power is off. In 2009, Hunger et al. proposed a new robotic system capable of positioning and inclining a needle within the same workspace as the manual template and accommodating existing seed dispensers.[14] In 2012, Jiang explored a 5-DOF hybrid-driven MR compatible robot for prostate brachytherapy.[15] It's composed of three stages structured by parallel mechanism and linked by a serial one. In 2014, Plitea et al. reported a parallel semi-automated robotic system with 5-DOFs for general brachytherapy compatible with CT scanners.[16] In 2016, a medical device that comprises a Kuka robot arm was developed. It's controllable in force and position. The 7-DOF system contains a needle bearing operating unit coupled to a 2D ultrasound probe, a camera and a supervision software.[17] A complete review of image-guided robotic brachytherapy can be found in the TG-192 report.[18] From the literature analysis, we remark that several developed robotic systems have more than 3-DOFs in order to adjust the position and the orientation of the needle according to the imaging system. However, having a needle insertion with more than 3-DOFs seems to be unrealistic for a clinical application since there is no treatment planning system capable to plan optimal dosimetry with complex needle trajectories. All needles are planned to be parallel to each other. Also, most of the robotics solution are heavy, bulky and not well adapted for a standard operating room (OR). In addition, such systems do not allow the surgeon to control the needle insertion raising an issue of acceptability by the clinicians.

A solution is proposed in this paper to overcome the issues found in the existing medical robots. Prostate brachytherapy procedure consists of the insertion of numerous needles within the prostate. Positions of these needles are calculated using the treatment planning system, which considers the needles as being all parallel to each other. Therefore, we developed a 3-DOF compact and lightweight robotic system as a preliminary work to evaluate the compatibility of such mechanisms with the clinical context. The mechanical design was inspired from the well-known delta parallel robot of Clavel.[23] The acceptability and the human–machine interaction issue were addressed by proposing a robot that allows comanipulation. Such a haptic device system has already been proven to assist medical interventions in areas such as neurosurgery,[22] orthopedic[20] or in urology[21] for prostate biopsies. But to the best of our knowledge, there is no haptic device designed for prostate brachytherapy to date. The aim of the proposed comanipulated robot (co-bot) is to replace the inaccurate grid template of 5 mm used in the standard procedure by an haptic guidance in order to help the surgeon in the positioning of the needles at the insertion entry point on the perineum.

https://doi.org/10.1017/S026357472000051X Published online by Cambridge University Press

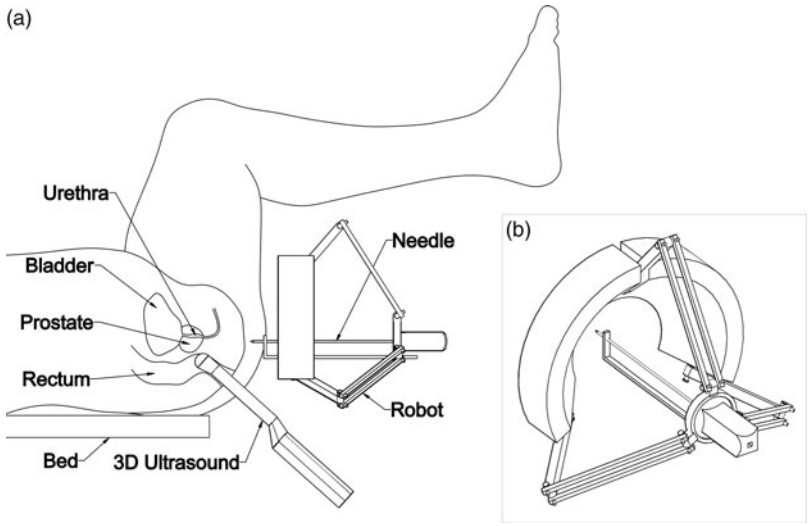

Fig. 1. Schematic description of the proposed parallel co-bot (a) in place during the brachytherapy procedure and (b) a detail view in 3D.

2. Robot Design

2.1. Mechanical design

Our solution aims to use a parallel robot since it is well suitable for an easy and fast installation in the OR; in addition, it offers safety which is in accordance with the medical procedure. This type of mechanism ensures direct link between the end effector and the base by a number of separate and independent linkages working simultaneously, which offers a better interaction between the surgeon and the robot. Moreover, parallel robots usually have components constructed with standardized units. Thus, they allow flexibility, variety in use and ease of maintenance. Our co-bot is a compact and lightweight system with consideration for the position of the TRUS probe and the patient (see Fig. 1(a)). The proposed design was inspired from the well-known delta robot model (3-DOFs). The Delta robot is composed of three pivot connections at the fixed base which allows to move the end effector. The system uses the principle of the four-bar mechanism to constrain the rotation of the end effector and allow it to be moved parallel to the fixed base. After, the parallelograms use ball joints to allow both a displacement in the axis of the corresponding pivot connection and also perpendicular thereto. We have adapted and parameterized the original Clavel's delta robot to best match the constraints of needle guidance in prostate brachytherapy procedure. More precisely, the parallel links are oriented to work horizontally; that's to say that the layout and working axis of the delta robot have been adapted to our context. Contrary to the usual use while the gravitational vector of the end effector is perpendicular to the plane containing the fixed base of the robot, in our design the gravitational vector is parallel to the plane containing the fixed base. Parallelograms links are used for retraction instead of extension compared to the standard delta robot. This permits to situate the workspace behind the robot basement, which is opened in order to access the patient perineum (see Fig. 1(a)). The proposed co-bot was designed as a haptic device. The co-bot end effector is now used by the surgeon to comanipulate the positioning and insertion of the needle in the prostate. As a result, we have adapted its design to allow a better grip (see Fig. 1(b)). The robot enhances the guidance through a force feedback provided by the motors. Each motor was directly linked to the main joint of each arm. A fixation system has also been designed to allow fixation on the operating table.

2.2. Kinematics

The kinematics of the proposed robot is adapted from the kinematics of the original delta robot.[24] All information about references frames and descriptions of the proposed robot are specified in Fig. 2. The kinematics of the robot is calculated in the Cartesian coordinate system $R_O(X, Y, Z)$ with the

https://doi.org/10.1017/S026357472000051X Published online by Cambridge University Press

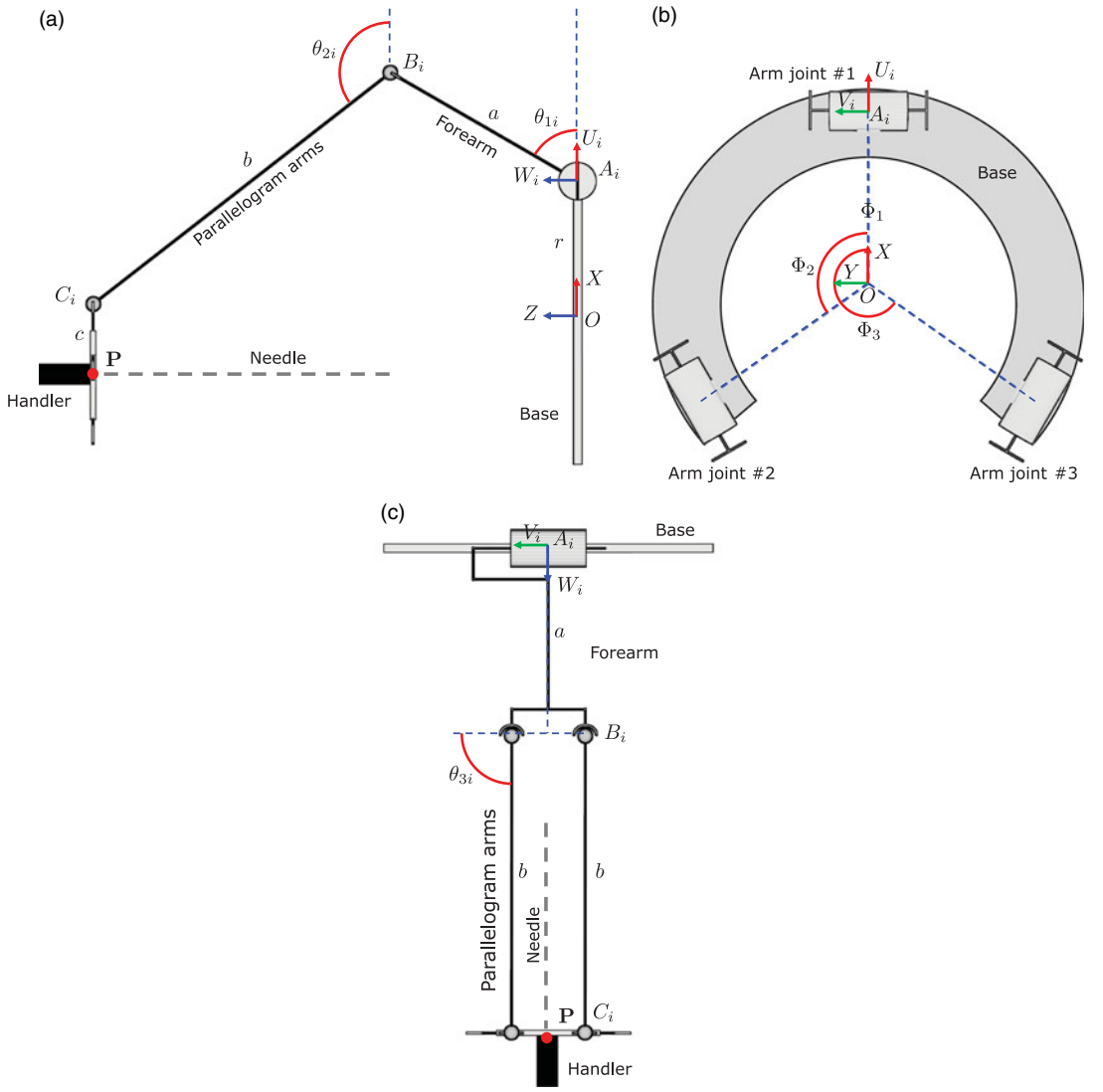

Fig. 2. (a) Left view, (b) front view and (c) top view of the reference frames for the different parts of the robot considering only the first arm.

origin O at the center of the robot base (see Fig. 2(b)). On each link $i \in \{1, 2, 3\}$, a local coordinate system is defined by $R_{A_i}(U_i, V_i, W_i)$ with origin A_i at the center of the first joint. The end effector, which is also used to handle the needle, is defined by the point $\mathbf{P} = (P_x, P_y, P_z)^T$ in the frame reference of R_O. This point may also be expressed in the coordinate of R_{A_i} as $(P_{U_i}, P_{V_i}, P_{W_i})^T$. The orientation ϕ_i of the link i is defined in the base plane (X, O, Y) and starting from (O, X) (see Fig. 2(b)). The proposed design has three links evenly distributed every 120°, then $\phi_1 = 0°$, $\phi_2 = 120°$ and $\phi_3 = 240°$.

2.2.1. Inverse kinematics. The pose of the robot end effector is obtained from the inverse kinematics detailed in this section. This is computed from the orientation θ_{1i} of joint A_i, θ_{2i} and θ_{3i} from the joint B_i for each link $i \in \{1, 2, 3\}$ (see Fig. 2(a) and (c)). We can express the pose of the end effector $\mathbf{P}$ from R_O to R_{A_i} as

$$\begin{bmatrix} P_{ui} \\ P_{vi} \\ P_{wi} \end{bmatrix} = \begin{bmatrix} \cos(\phi_i) & \sin(\phi_i) & 0 \\ -\sin(\phi_i) & \cos(\phi_i) & 0 \\ 0 & 0 & 1 \end{bmatrix} \begin{bmatrix} P_x \\ P_y \\ P_z \end{bmatrix} + \begin{bmatrix} -r \\ 0 \\ 0 \end{bmatrix} \tag{1}$$

https://doi.org/10.1017/S026357472000051X Published online by Cambridge University Press

in addition **P** may also be defined by,

$$\begin{bmatrix} P_{ui} \\ P_{vi} \\ P_{wi} \end{bmatrix} = \begin{bmatrix} a.\cos(\theta_{1i}) - c + b.\sin(\theta_{3i}).\cos(\theta_{2i}) \\ b.\cos(\theta_{3i}) \\ a.\sin(\theta_{1i}) + b.\sin(\theta_{3i}).\sin(\theta_{2i}) \end{bmatrix} \tag{2}$$

where a, b and c are the lengths of the links (see Fig. 2(a) and (c)). A first angle θ_{3i} can be extracted from (2):

$$\theta_{3i} = \pm \arccos\left(\frac{P_{vi}}{b}\right) \tag{3}$$

This leads to two possible solutions for θ_{3i}. A second angle θ_{1i} is calculated by isolating θ_{2i} in (2) from P_{ui} and P_{wi} equations. Then, the two resulting equations are squared and summed:

$$(c + P_{ui})^2 + P_{wi}^2 + a^2 - 2a(P_{ui} + c).\cos(\theta_{1i}) - 2aP_{wi}.\sin(\theta_{1i}) = b^2.(\sin(\theta_{3i}))^2 \tag{4}$$

In order to calculate θ_{1i}, $\sin(\theta_{1i})$ and $\cos(\theta_{1i})$ from (4) are replaced by the half-angle tangent defined as follows:

$$\omega_{1i} = \tan\left(\frac{\theta_{1i}}{2}\right) \tag{5}$$

This lead to a final equation which can be rewritten by the following canonical form:

$$A.\omega_{1i}^2 + B.\omega_{1i} + C = 0 \tag{6}$$

where

$$\begin{bmatrix} A \\ B \\ C \end{bmatrix} = \begin{bmatrix} P_{wi}^2 + P_{ui}^2 + 2c.P_{ui} + 2a.P_{ui} + a^2 + c^2 - b^2\sin^2(\theta_{3i}) + 2ac \\ -4a.P_{wi} \\ P_{wi}^2 + P_{ui}^2 + 2c.P_{ui} - 2a.P_{ui} + a^2 + c^2 - b^2\sin^2(\theta_{3i}) - 2ac \end{bmatrix} \tag{7}$$

By resolving (7), two values of ω_{1i} can be found, corresponding to the two distinct values of θ_{1i}. On the other hand, the two solutions of θ_{1i} are independent of the two solutions of θ_{3i} in (3). Combining the θ_{1i} and θ_{3i} solutions leads to four possible solutions. For each solution, a single value of θ_{2i} can be obtained. Given θ_{1i} and θ_{3i}, θ_{2i} can be found by isolating, respectively, $\cos(\theta_{2i})$ and $\sin(\theta_{2i})$ in (2) from P_{ui} and P_{wi} equations. Due to the geometry of the co-bot, the set of the four solutions corresponds to only two distinct configurations of each link. In case of the prostate brachytherapy, the proposed co-bot will be constrained to operate only in the poses where $0 < \theta_{2i} < \pi$ and $0 < \theta_{3i} < \pi$.

2.2.2. Direct kinematics. The direct kinematics gives the coordinates $(P_x, P_y, P_z)^T$ of the end effector for given joint values $\{\theta_{11}, \theta_{12}, \theta_{13}\}$. Geometrically speaking, the direct kinematics solution correspond to the intersection of the three spheres obtained by all possible end effector positions for each link considered separately. The equation that describes a sphere associated to the link i is written as follows:

$$\begin{aligned} b^2 = {} & P_x^2 + P_y^2 + P_z^2 - 2a.P_z - 2P_x.\cos(\phi_i)(a.\cos(\theta_{1i}) + r - c) \\ & - 2P_y.\sin(\phi_i)(a.\cos(\theta_{1i}) + r - c) + (a.\cos(\theta_{1i}) + r - c)^2 + (a.\sin(\theta_{1i}))^2 \end{aligned} \tag{8}$$

Intersection between the two spheres described by the links 1 and 2 is obtained by subtracting Eq. (8) with $i = 1$ and the same equation with $i = 2$:

$$q_{12}.P_x + k_{12}.P_y + s_{12}.P_z + t_{12} = 0 \tag{9}$$

https://doi.org/10.1017/S026357472000051X Published online by Cambridge University Press

where

$$\begin{bmatrix} q_{12} \\ k_{12} \\ s_{12} \\ t_{12} \end{bmatrix} = \begin{bmatrix} 2\cos(\phi_2).(a.\cos(\theta_{12}) + r - c) - 2\cos(\phi_2).(a.\cos(\theta_{11})) - 2\cos(\phi_1).(r - c) \\ 2\sin(\phi_2).(a.\cos(\theta_{12}) + r - c) - 2\sin(\phi_2).(a.\cos(\theta_{11})) - 2\sin(\phi_1).(r - c) \\ 2a.\sin(\theta_{12}) - 2a.\sin(\theta_{11}) \\ (a.\cos(\theta_{11}) + r - c)^2 + (a.\sin(\theta_{11}))^2 - (a.\sin(\theta_{12}))^2 - (a.\cos(\theta_{12}) + r - c)^2 \end{bmatrix} \tag{10}$$

The same intersection between the two spheres provided by arms 1 and 3 can be calculated:

$$q_{13}.P_x + k_{13}.P_y + s_{13}.P_z + t_{13} = 0 \tag{11}$$

A system of linearly independent equations can be derived from (9) and (10). The resulting equations define a line where the direct kinematic solution may exist. The direct kinematic solutions correspond to the intersection of this line with one of the three spheres, representing the possible Cartesian positions of the end effector in our reference frame. This is done by first expressing P_y and P_z in terms of P_x from Eq. (11), and then substituting the resulting expressions in (8) for $i = 1$. The final equation can be expressed as follows:

$$m_0 P_x^2 + m_1 P_x + m_2 = 0 \tag{12}$$

where

$$\begin{bmatrix} m_0 \\ m_1 \\ m_2 \end{bmatrix} = \begin{bmatrix} 1 + \frac{n_1^2}{n_2^2} + \frac{n_4^2}{n_5^2} \\ \frac{2.n_0.n_1}{n_2^2} + \frac{2.n_3.n_4}{n_5^2} - 2.n_6.\cos(\phi_1) - \left(\frac{2a.n_4}{n_5}\right).\sin(\theta_{11}) - \left(\frac{2.n_6.n_1}{n_2}\right).\sin(\phi_1) \\ n_6^2 - b^2 + \frac{n_0^2}{n_2^2} + \frac{n_3^2}{n_5^2} + (a.\sin(\theta_{11}))^2 - \left(\frac{2n_0.n_6}{n_2}\right).\sin(\phi_1) - \left(\frac{2.a.n_3}{n_5}\right).\sin(\theta_{11}) \end{bmatrix} \tag{13}$$

with

$$\begin{bmatrix} n_0 \\ n_1 \\ n_2 \\ n_3 \\ n_4 \\ n_5 \\ n_6 \end{bmatrix} = \begin{bmatrix} s_{12}.t_{13} - s_{13}.t_{12} \\ q_{13}.s_{12} - q_{12}.s_{13} \\ k_{12}.s_{13} - k_{13}.s_{12} \\ k_{13}.t_{12} - k_{12}.t_{13} \\ q_{12}.k_{13} - q_{13}.k_{12} \\ k_{12}.s_{13} - k_{13}.s_{12} \\ a.cos(\theta_{11}) + r - c \end{bmatrix} \tag{14}$$

Once Eq. (12) is resolved using the q, k, s, t values from (10) and P_x found, P_y and P_z can be obtained using back substitution in (9) and (10). Finally, we are able to calculate the Cartesian coordinates $(P_x, P_y, P_z)^T$ from the joint coordinate $\{\theta_{11}, \theta_{12}, \theta_{13}\}$.

2.3. Jacobian and singularities

2.3.1. Jacobian of the manipulator. The robot Jacobian defines the relationship between the velocity of the end effector in the Cartesian (or task) space to the actuated joint velocities in joint space:

$$\dot{\boldsymbol{\theta}} = \boldsymbol{J}\dot{\boldsymbol{P}} \tag{15}$$

where $\dot{\boldsymbol{\theta}}$ is a vector that represents the actuated joints velocities, $\dot{\boldsymbol{P}}$ is a vector that represents the velocity of the end effector and $\mathbf{J}$ is, in this case, the (3×3) Jacobian matrix. The relation between $\dot{\boldsymbol{\theta}}$ and $\dot{\boldsymbol{P}}$, as demonstrated in the work,[25] can be rewritten as follows:

$$\boldsymbol{J_F}\dot{\boldsymbol{P}} + \boldsymbol{J_I}\dot{\boldsymbol{\theta}} \tag{16}$$

where $\boldsymbol{J_F}$ is the direct Jacobian and $\boldsymbol{J_I}$ is the inverse Jacobian. Both matrices will be used to study the direct and inverse kinematic singularities. In order to estimate these matrices, a vector approach

https://doi.org/10.1017/S026357472000051X Published online by Cambridge University Press

is used as follows:

$$\overrightarrow{\boldsymbol{OP}} = \overrightarrow{\boldsymbol{OA_i}} + \overrightarrow{\boldsymbol{A_iB_i}} + \overrightarrow{\boldsymbol{B_iC_i}} + \overrightarrow{\boldsymbol{C_iP}} \tag{17}$$

The vector from the robot origin $\boldsymbol{O}$ to the end effector $\boldsymbol{P}$ is written in Eq. (17) and this equation is differentiated and expressed in the coordinate frame $R_{A_i}(U_i, V_i, W_i)$:

$$\boldsymbol{V}_{\boldsymbol{P}(\boldsymbol{R}_{\boldsymbol{A_i}})} = \overrightarrow{\boldsymbol{W}_{\boldsymbol{A_iB_i}}} \wedge \overrightarrow{\boldsymbol{A_iB_i}} + \overrightarrow{\boldsymbol{W}_{\boldsymbol{B_iC_i}}} \wedge \overrightarrow{\boldsymbol{B_iC_i}} \tag{18}$$

where $\overrightarrow{\boldsymbol{W}_{\boldsymbol{A_iB_i}}}$ and $\overrightarrow{\boldsymbol{W}_{\boldsymbol{B_iC_i}}}$ are, respectively, the angular velocity of the joint B_i with respect to the joint A_i and the joint C_i with respect to the joint B_i of the arm i in the coordinate frame $R_{A_i}(U_i, V_i, W_i)$. $\dot{\boldsymbol{P}}(\boldsymbol{R}_{\boldsymbol{A_i}}) = (\dot{P}_{U_i}, \dot{P}_{V_i}, \dot{P}_{W_i})^T$ is the velocity of the end effector in the coordinate frame $R_{A_i}(U_i, V_i, W_i)$ in Eq. (18).

The presence of $\overrightarrow{\boldsymbol{W}_{\boldsymbol{B_iC_i}}}$ in Eq. (18) introduces an undesired dependence with $\dot{\theta}_{2i}$ and $\dot{\theta}_{3i}$. In order to get rid of that, the scalar product of Eq. (18) is achieved using the unit vector:

$$\overrightarrow{\boldsymbol{b_i}} = \frac{1}{\left\| \overrightarrow{\boldsymbol{B_iC_i}} \right\|} . \overrightarrow{\boldsymbol{B_iC_i}} \tag{19}$$

leading to the equation

$$\overrightarrow{\boldsymbol{b_i}} . \dot{\boldsymbol{P}}(\boldsymbol{R}_{\boldsymbol{A_i}}) = \overrightarrow{\boldsymbol{b_i}} . (\overrightarrow{\boldsymbol{W}_{\boldsymbol{A_iB_i}}} \wedge \overrightarrow{\boldsymbol{A_iB_i}}) \tag{20}$$

with

$$\overrightarrow{\boldsymbol{b_i}} = \begin{bmatrix} \sin(\theta_{3i}).\cos(\theta_{2i}) \\ \cos(\theta_{3i}) \\ \sin(\theta_{2i}).\sin(\theta_{3i}) \end{bmatrix} \tag{21}$$

$$\overrightarrow{\boldsymbol{W}_{\boldsymbol{A_iB_i}}} = \begin{bmatrix} 0 \\ -\theta_{1i} \\ 0 \end{bmatrix} \tag{22}$$

and

$$\overrightarrow{\boldsymbol{A_iB_i}} = \begin{bmatrix} a.\cos(\theta_{1i}) \\ 0 \\ a.\sin(\theta_{1i}) \end{bmatrix} \tag{23}$$

The velocity of the end effector $\dot{\boldsymbol{P}}(\boldsymbol{R}_{\boldsymbol{A_i}})$ can be calculated by replacing expressions from Eqs. (21)–(23) into Eq. (20). Then, the resulting equation is transformed from the coordinate frame R_{A_i} to the Cartesian coordinate system R_O using Eq. (1). This calculation is done for each link $i = \{1, 2, 3\}$. The resulting expressions are arranged to obtain the form

$$\boldsymbol{J_I} \begin{bmatrix} \dot{\theta_{11}} \\ \dot{\theta_{12}} \\ \dot{\theta_{13}} \end{bmatrix} = \boldsymbol{J_F} \begin{bmatrix} \dot{P}_X \\ \dot{P}_Y \\ \dot{P}_Z \end{bmatrix} \tag{24}$$

where, $\dot{\boldsymbol{P}}(\boldsymbol{R_O}) = (\dot{P}_X, \dot{P}_Y, \dot{P}_Z)^T$ is the velocity of the end effector in the coordinate system R_O, and $\dot{\theta}_{11}$, $\dot{\theta}_{12}$ and $\dot{\theta}_{13}$ represent, respectively, the angular velocities of the main base joint A_i for arms 1, 2 and 3. Finally, the direct and the inverse Jacobian of the proposed co-bot are

$$\boldsymbol{J_F} = \begin{bmatrix} J_{F_{11}} & J_{F_{12}} & J_{F_{13}} \\ J_{F_{21}} & J_{F_{22}} & J_{F_{23}} \\ J_{F_{31}} & J_{F_{32}} & J_{F_{33}} \end{bmatrix} \tag{25}$$

https://doi.org/10.1017/S026357472000051X Published online by Cambridge University Press

$$\boldsymbol{J_I} = \begin{bmatrix} J_{I_1} & 0 & 0 \\ 0 & J_{I_2} & 0 \\ 0 & 0 & J_{I_3} \end{bmatrix} \tag{26}$$

and each element of these two matrices can be calculated as follows:

$$J_{F_{i1}} = \cos(\phi_i).\cos(\theta_{2i}).\sin(\theta_{3i}) - \sin(\phi_i).\cos(\theta_{3i}) \tag{27}$$

$$J_{F_{i2}} = \sin(\phi_i).\cos(\theta_{2i}).\sin(\theta_{3i}) - \cos(\phi_i).\cos(\theta_{3i}) \tag{28}$$

$$J_{F_{i3}} = \sin(\theta_{3i}).\sin(\theta_{2i}) \tag{29}$$

$$J_{I_i} = a.\sin(\theta_{3i}).\sin(\theta_{2i} - \theta_{1i}) \tag{30}$$

where $i = \{1, 2, 3\}$ is the column index of both matrices.

2.3.2. Singularities. The main interest of calculating the robot Jacobian is to have the capability to determine the singularities of the co-bot. This will be used for optimizing the co-bot design by moving singularity configurations outside the workspace. The singularity can be mathematically expressed as the robot configurations where the determinant of $\boldsymbol{J_F}$ is equal to 0, leading to the following expressions:

$$\sin(\theta_{31}).\sin(\theta_{21}) = 0 \tag{31}$$

$$\sin(\theta_{32}).\sin(\theta_{22}) = 0 \tag{32}$$

$$\sin(\theta_{23}).\sin(\theta_{33}) = 0 \tag{33}$$

The proposed co-bots have singularity positions when $\theta_{2i} = \{0, \pi\}$ or $\theta_{3i} = \{0, \pi\}$ for all of the three links. In terms of geometry, one singularity occurs when the forearm and the parallelogram link are coplanar with the end effector. Another singularity corresponds when two of the three links are parallel to each other. The inverse kinematic singularities $\boldsymbol{J_I}$ occur when $\theta_{1i} - \theta_{2i} = \{0, \pi\}$ or $\theta_{3i} = \{0, \pi\}$. This corresponds to a condition when the forearm and the parallelogram link of the same kinematic chain are coplanar.

2.4. Design optimization

From to the robot kinematics, the same set of angles $(\theta_{11}, \theta_{12}, \theta_{13})$ can result in two different poses of the end effector $\boldsymbol{P}$. The dimensions of the links should be carefully chosen so as to avoid singular configurations within the workspace and ensure a more stable control of the co-bot. To get an optimal design, we need to search for the optimal geometric configuration according to objective functions and geometric constraints. Most of the time, an optimal design problem should follow the relationships described in the following:

$$\begin{aligned} &\text{Find a vector } A = [a_1, a_2, ..., a_n] \\ &\text{that minimize: } B(A) = [b_1(A), b_2(A), ..., b_n(A)] \\ &\text{with } C_m(A) \leqslant 0 \text{ (inequality constraints)} \\ &\text{and } D_h(A) = 0 \text{ (equality constraints)} \end{aligned} \tag{34}$$

Here A is the vector of design parameters, B is the vector of the considered performance criteria within the optimal design issue and C and D are the geometric constraints.

For our problematic, a volume of 55 mm × 55 mm × 120 mm was defined as workspace function. The dimensions of 55 mm × 55 mm correspond to the conventional template size that covers the prostate area in brachytherapy.[26] The dimension of 120 mm is the maximum distance of the needle insertion, which was estimated by measuring the distance between the perineum and the prostate apex using patient CT. This value was also confirmed by measuring depth of insertion on needle during brachytherapy procedure.

https://doi.org/10.1017/S026357472000051X Published online by Cambridge University Press

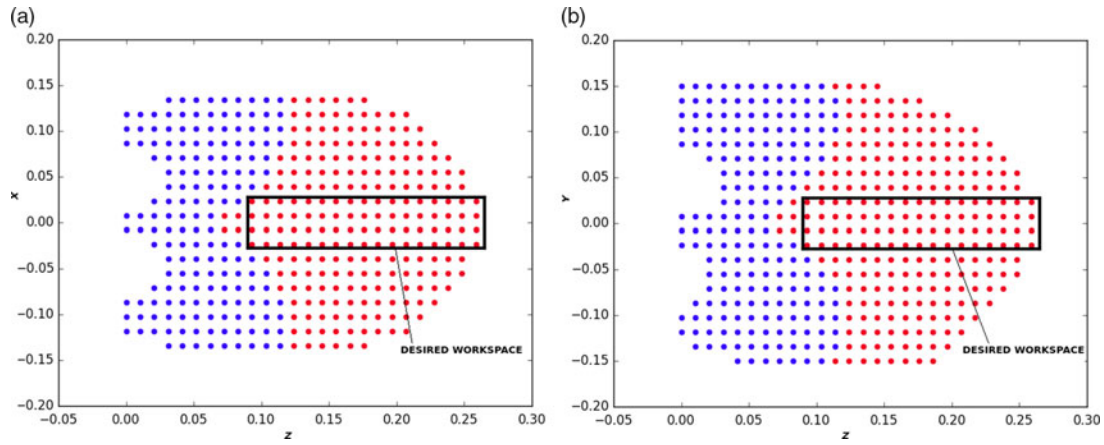

Fig. 3. Central cross section of the distribution of the possible positions of the co-bot using the final set of dimensions for (a) the plane (xOz), which is the left view, and (b) the plane (yOz), which is the top view. The points in red correspond to the positions that satisfy the geometric constraints and the blue ones the positions that are unsustainable.

The geometric constraints for each link are

$$0 < \theta_{2i} < \pi \tag{35}$$

$$\theta_{2i} > \theta_{1i} \tag{36}$$

An iterative algorithm written in Python was used to find the best dimensions of the robot links. This is done by using a sample of 600 end effector poses uniformly distributed within a region of interest 300 mm × 300 mm × 300 mm centered on the workspace. For each of this pose, the inverse kinematics was computed to determine the set of joint angles (θ_{11}, θ_{12}, θ_{13}). These values are subsequently tested using the previous established geometric constraint in order to know if the configuration is possible or not. Several solutions that satisfy the different constraints were found. However, the solution that corresponds to the most compact system was selected ($a = 120$ mm, $b = 150$ mm, $r = 86.6$ mm, $c = 43.3$ mm). In order to ensure that there is no collision between mechanical parts for the optimized set of dimensions, a simulation is performed using Onshape[27] software. The resulting plot that shows the possible and the unwanted configurations for the final set of dimensions selected are shown on Fig. 3. This plot shows a desired workspace located within a volume that has no singularities.

2.5. Mechanical realization of the co-bot

A prototype of the co-bot has been realized to evaluate practically the adequacy of the proposed solution with the prostate brachytherapy procedure. During the mechanical realization, a special emphasis was placed on the choice of the bearings used at the joints. To limit friction and to offer a smooth guiding sensation for the operator who comanipulates, we used ball bearings with plastic rings. In addition, for the same reasons and to avoid irreversibility issues that can occur for high reduction ratio, we chose not to use gearmotors. As it can be seen on Fig. 4, the end effector was designed as a half dome to facilitate the gripping by the operator. Moreover, this choice of the design allows to advance the attachment system. Thus, it allows at least an insertion up to 125 mm for a needle of about 200 mm in length. However, after testing the prototype, we recognized that a mechanism for maintaining the stability of the needle while inserting it in the prostate should be added to the co-bot. Our prototype is quite compact. Its maximum footprint can be delimited by a cube of 350 mm of side. Moving parts of the co-bot prototype weighs only 450 g. This is an advantage considering the fact that we are in a context of comanipulation.

3. Evaluation Studies

3.1. Resolution at the end effector

In order to evaluate the design of the co-bot, we have studied the theoretical resolution at the end effector. The aim is ensuring that the system is capable of meeting the resolution needed for the

https://doi.org/10.1017/S026357472000051X Published online by Cambridge University Press

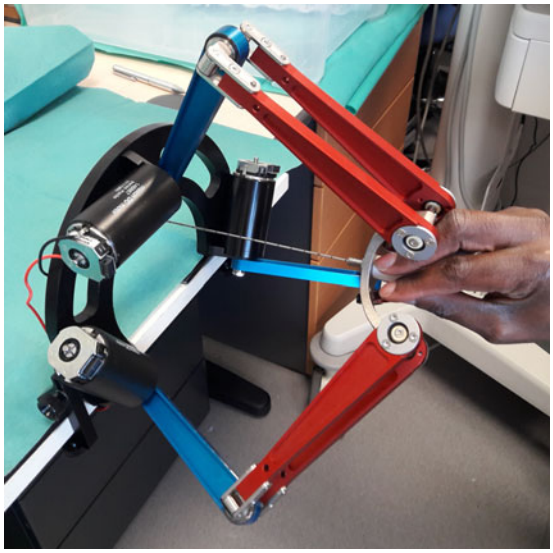

Fig. 4. Realization of the co-bot.

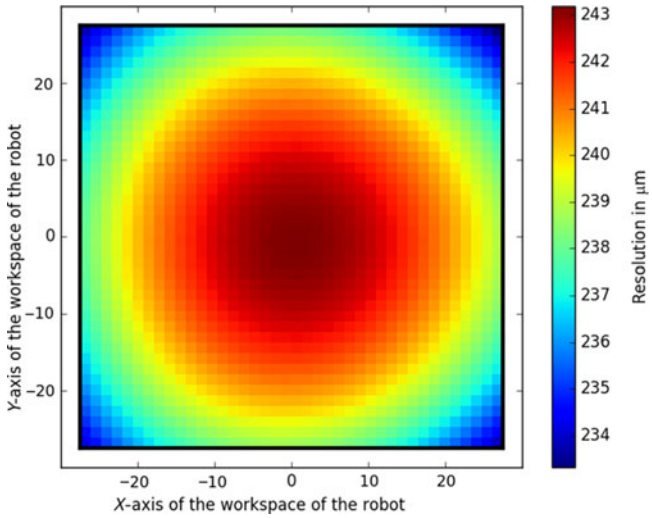

Fig. 5. Resolution at the end effector considering classical encoder values of 12 bits and a position of the end effector at $z = 120$ mm from the robot base (i.e. tip of the needle closes to the perineum).

brachytherapy prostate surgery. The resolution of the end effector is the smallest displacement, d, that can be done from the point $\boldsymbol{P}$ in the workspace of the co-bot. This value was calculated by using the smallest rotation angle that can be measured by the encoder of the articular joints. This is depends on the number of bits of the encoder and can be calculated using

$$r_\theta = \frac{2\pi}{2^n - 1} \tag{37}$$

For each possible pose $\boldsymbol{P}$ in the workspace, the joint angles $\boldsymbol{\theta}$ are calculated from the inverse kinematics. Then, the smallest angular rotation r_θ is applied to this joint angle leading to an increase in the joint values $\boldsymbol{\theta'} = \boldsymbol{\theta} + r_\theta$. The new joint angles are converted back to the Cartesian workspace by direct kinematics to provide the new position $\boldsymbol{P'}$. The final resolution is subsequently obtained by calculating the Euclidean distance between the point $\boldsymbol{P}$ and $\boldsymbol{P'}$. The results obtained when considering the classical encoder values of 12 bits and a position of the end effector at $z = 120$ mm from the robot base (i.e. tip of the needle on the perineum) are plotted on Fig. 5.

The resolution is almost constant within the workspace, since the values range between 0.23 and 0.25 mm. This may be an advantage considering that in comanipulation, homogeneous resolution will

https://doi.org/10.1017/S026357472000051X Published online by Cambridge University Press

lead to a smooth control between the movement of the end effector. The largest resolution calculated was 0.25 mm, which is enough considering that in brachytherapy procedure, an accuracy within <4 mm is sufficient.[19]

3.2. Force analysis at the end effector

To evaluate the performance of the proposed robot during comanipulation, the isotropic force capability at the end effector was estimated for the entire workspace. The isotropic force is the highest force that can be applied simultaneously in all directions at the end effector. This value depends on the maximum torque $\Gamma_{\max}$ applied by the active joint A_i of each link. Since three motors are used, one for each link, the maximum torque vector is $\boldsymbol{\Gamma} = [\Gamma_1, \Gamma_2, \Gamma_3]^T$ and each motor delivers a torque in the range $-\Gamma_{\max} \leq \Gamma_i \leq \Gamma_{\max}$. For each possible torque vector $\boldsymbol{\Gamma}$, the corresponding isotropic forces vector $\boldsymbol{F}(\boldsymbol{R_O}) = [F_X, F_Y, F_Z]^T$ was computed as follows:

$$\boldsymbol{F} = (\boldsymbol{J}^T)^{-1}.\left(\boldsymbol{\Gamma} + \boldsymbol{\Gamma_{fc}}\right) \tag{38}$$

where $\boldsymbol{\Gamma_{fc}}$ is the torque vector induced by friction in the joints and $\boldsymbol{J}$ is the Jacobian matrix of the co-bot obtained using the relation

$$\boldsymbol{J} = (\boldsymbol{J_I})^{-1}\boldsymbol{J_F} \tag{39}$$

To model the torque induced by friction in the joints of the co-bot, we will consider the Coulomb friction model.[30] The friction torque is applied in the opposite sense of the motion and is proportional to the load in the joint:

$$\boldsymbol{\Gamma_{fc}} = \boldsymbol{F_c}.[\boldsymbol{sgn}(\boldsymbol{q_1}), \boldsymbol{sgn}(\boldsymbol{q_2}), \boldsymbol{sgn}(\boldsymbol{q_3})]^T, \quad q_j \neq 0 \, for \, 0 \leq j \leq 2 \tag{40}$$

where q_j is the velocity in the joint j and $\boldsymbol{F_c}$ is the Coulomb force computed by

$$\boldsymbol{F_c} = \zeta.\boldsymbol{Q} \tag{41}$$

with ζ the friction coefficient and $\boldsymbol{Q}$ the load vector in the joints. However in Eq. (40), the Coulomb friction torque is not defined when the velocity q_j in a joint j is equal to zero. To overcome this issue, we can consider for simulation purpose that $\Gamma_{fc} = 0$ when the velocity in the joint is equal to zero. To enhance stability when modeling Coulomb friction torque, it is usual to consider instead a dead zone around the zero velocity, where the Coulomb friction torque will be neglected (equal to zero). A more complex and effective way to compute the friction torque that considers the case when velocity in the joint is null is the Karnopp friction model.[29] However for our co-bot in the context of prostate brachytherapy assistance, friction torques in the joints can be safely neglected for the following reasons. Firstly, we used commercial low-friction joints like ball bearing and low friction rings. Secondly, the motors used for the design of the co-bot are DC motors. Unlike harmonic drives such as AC motors, in which friction torque can be of high magnitude, friction torque in DC motors are generally of low magnitude. Moreover, the co-bot is not designed to support high loads. For all these reasons, to model the force capacity of our co-bot, $\boldsymbol{\Gamma_{fc}}$ in Eq. (38) will be considered equal to null vector.

The Jacobian matrix $\boldsymbol{J}$ in Eq. (38) is calculated for a given end effector pose $\boldsymbol{P}$ in 3D space, by computing the joint angles $\boldsymbol{\theta}$ given a pose using inverse kinematics. Thus, the isotropic force vector can be estimated for every possible end effector pose within the workspace. This is calculated using

$$F_{iso}(\boldsymbol{P}) = \max_{\forall \boldsymbol{\Gamma}} (\min \boldsymbol{F}(\boldsymbol{P}, \boldsymbol{\Gamma})) \tag{42}$$

The final isotropic force value F_{iso} is the maximum force encountered considering every possible torques vector of the smallest value in $\{F_X, F_Y, F_Z\}$. An evaluation study is performed using motors with a maximal torque values of 4 Nm. The results for isotropic forces at a distance of $z = 120$ mm from the robot base (i.e. tip of the needle on the perineum) are plotted on Fig. 6(a).

The results show that the isotropic force ranges from 11.5 N to reach 28 N, which is enough to compensate for the weight of the co-bot links and for end effector guidance during the positioning of the needle. The mass of all the moving parts of the robot was estimated to be 450 g. However, considering the minimum isotropic force of 11.5 N, it seems insufficient for performing an insertion where the needle needs to cross the perineum. This task requires a force that can reach 17 N.[26] We

https://doi.org/10.1017/S026357472000051X Published online by Cambridge University Press

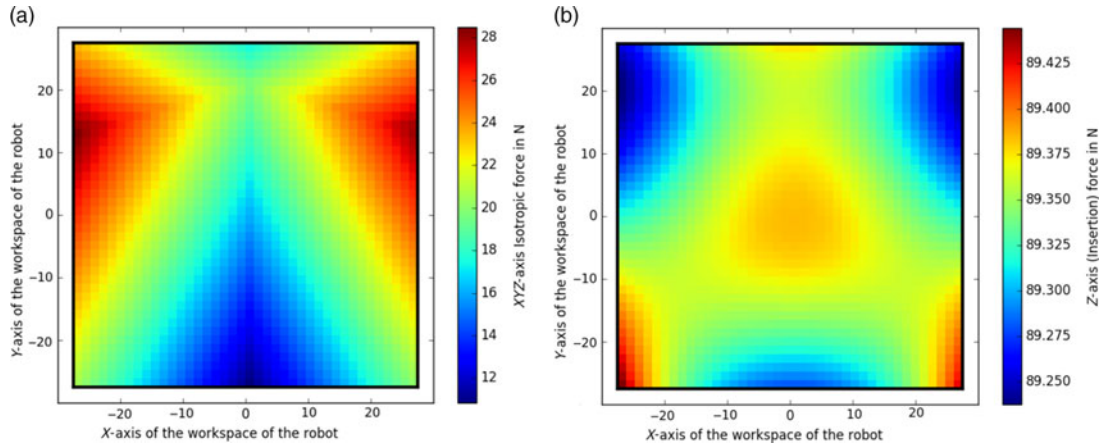

Fig. 6. (a) Front view (plane xOy) of the isotropic force for a distance end effector/base of 120 mm, (b) maximum force along the z-axis (needle insertion axis) for the top view (plane yOz).

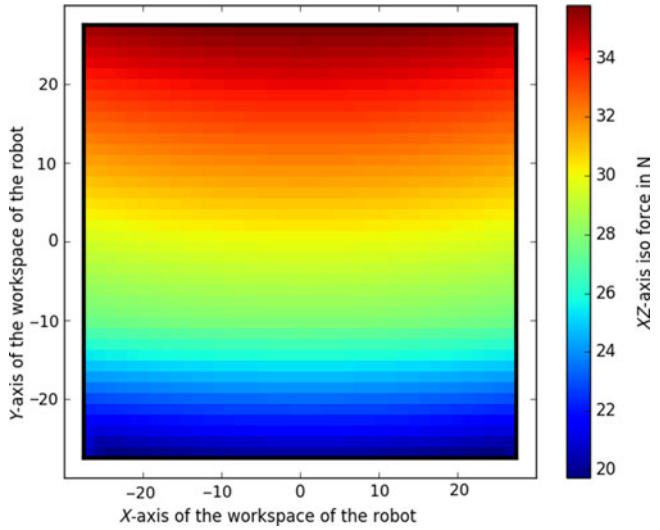

Fig. 7. Force along x- and z-axes at end effector of the cobot for a distance end effector/base of 120 mm.

note in a previous work,[28] that the positioning of the needle at the entry point of the perineum and the insertion of the needle in the prostate are two decoupled tasks. This implies that while inserting the needle into the perineum (along the z-axis), the co-bot does not have to provide force guidance for positioning in the x- and y-axes. In order to confirm the capability in force of the robot along the insertion axis (z-axis), the insertion force was estimated using

$$F_{in}(\boldsymbol{P}) = \max_{\forall \boldsymbol{\Gamma}} F_Z(\boldsymbol{P}, \boldsymbol{\Gamma}) \tag{43}$$

On Fig. 6(b), the insertion forces are plotted considering a distance of $z = 120$ mm from the robot base (i.e. tip of the needle on the perineum). The results show that the insertion forces considering only the z-axis (meaning that the force in x- and y-axes is equal to zero) were almost constant with a value around 89 N. This value is purely theoretical, since the co-bot must counter its weight in the gravity axis (x-axis in our case). The force that can be provided by our co-bot simultaneously in x- and z-axes was estimated as follows:

$$F_{xz}(\boldsymbol{P}) = \max_{\forall \boldsymbol{\Gamma}} \left(\min\left(\boldsymbol{F_x}(\boldsymbol{P}, \boldsymbol{\Gamma}), \boldsymbol{F_z}(\boldsymbol{P}, \boldsymbol{\Gamma})\right)\right) \tag{44}$$

As we can see on Fig. 7, the co-bot can now provide a force between 20 and 36 N in x- and z-axes simultaneously, which is enough for compensating for the co-bot's gravity while providing guidance

https://doi.org/10.1017/S026357472000051X Published online by Cambridge University Press

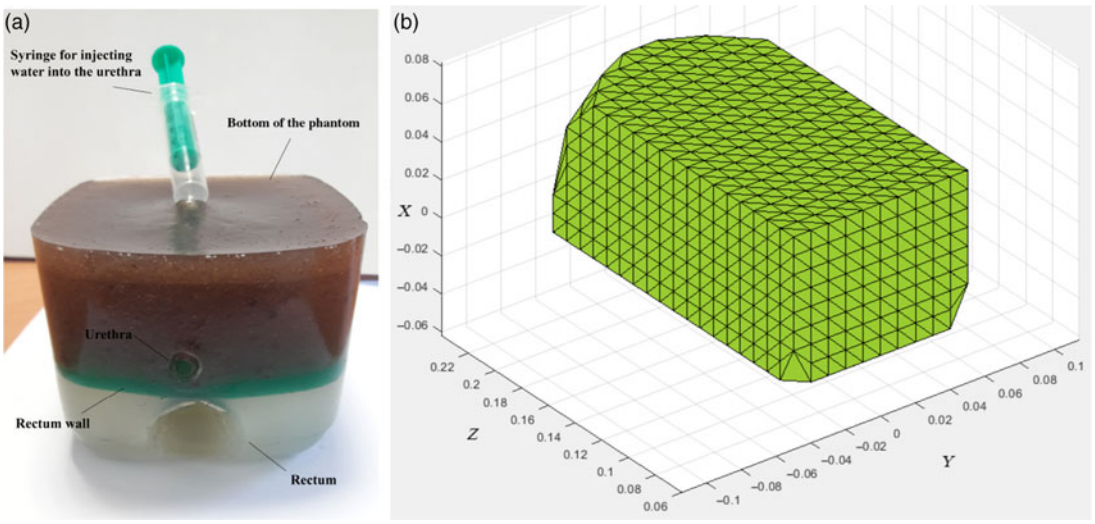

Fig. 8. (a) Homemade PVC prostate phantom used for the experimental evaluations. (b) Workspace volume of the co-bot estimated with the depth camera and considering the TRUS probe in place.

during the insertion of the needles in the prostate. This confirms the capability of the proposed co-bot to help in insertion the needle through the perineum, a task that requires less than 17 N.

3.3. Experimental evaluation

In order to evaluate the proposed co-bot and its compatibility in brachytherapy context, an experimental bench was realized. This experimental evaluation consists in the use of a depth camera, TRUS probe and a prostate phantom. The aim is to estimate the co-bot workspace while the TRUS probe is in place inside the rectum phantom. As depth camera, a Kinect 2 was used with the software GML C ++ camera calibration toolbox,[31] in order to estimate in 3D the position of the end effector of the robot. The prostate phantom is a gelatinous structure, based on thermoplastic polymer polyvinyl chloride (PVC), reproducing some of the mechanical properties and ultrasound imaging of the prostate. Based on medical images from magnetic resonance imaging (MRI) system, we build a realistic phantom that considers urethra and rectum (see Fig. 8(a)). Two measures of the workspace were performed with the depth camera, one without the TRUS and one with the TRUS inside the rectum phantom. The co-bot was manipulated to reach its displacement limits in every direction. Each time a measurement of the 3D coordinate of the end effector with the GML software and the camera was performed. The first workspace, without the TRUS probe, has led a volume corresponding to a square base rectangular parallelepiped of dimension (100 mm × 100 mm × 240 mm) centered in the center of the co-bot. This volume was compatible with the requirement in prostate brachytherapy; however, the volume is smaller of 13% of the estimated volume obtained by the calculation. This can be explained by the fact that the constraints imposed by the parallel architecture of the co-bot limit the amplitude of motors rotation. The measure workspace with the TRUS probe inside the phantom is shown on Fig. 8(b). In this case, the measured volume was drastically reduced due to the collision of the co-bot and the US probe. However, the achievable volume was 71 mm × 100 mm × 240 mm, which is still compatible with the medical application since the desired volume was (55 mm × 55 mm × 120 mm).

4. Conclusion and Future Work

In this paper, we present a delta robot for comanipulated application in prostate brachytherapy assistance. The aim was to estimate if this design may help the surgeon of placing accurately the needle at the right position before the insertion through the perineum. In the standard procedure, a template grid with holes of 5 mm spacing is used as helper to approximately place the needle at the perineum entry point. The proposed co-bot will accurately perform this step conjointly with the surgeon without any grid template. The surgeon completely controls the insertion (forward and backward), thereby allowing for a better safety and acceptability of the system in the OR. The guidance may

https://doi.org/10.1017/S026357472000051X Published online by Cambridge University Press

be still activated while the needle is inserted through the perineum in order to keep the trajectory as straight as possible. The 3-DOFs of the proposed robot is sufficient for the application since treatment planning system does not provide complex needle trajectory. The results show that the co-bot can reach a resolution of 0.25 mm, which is an improvement compared to the conventional procedure where seeds are inserted manually using a 5-mm grid template and TRUS image guidance. However, further experimental evaluations are needed to estimate in practice the real resolution, but the results are promising. A parallel architecture is adopted for the mechanical design of the co-bot (delta robot) in order to obtain a compact design. The co-bot is designed to fit within a cube of 300 mm × 300 mm × 300 mm. The co-bot is lightweight with a mass of 2.5 kg including the motors. This is an advantage considering the targeted use in the OR, where the system has to be moved, attached and detached to the surgical couch easily and quickly. The kinematics and singularities of the co-bot were calculated in order to optimize the workspace while taking its medical application into account. These calculations were also used to evaluate the theoretical capability of the proposed robot. The final workspace estimated experimentally was compatible for a real medical application in prostate brachytherapy context.

The isotropic forces at the co-bot end effector are dependent on the maximum torques of the motor. Our evaluation shows a minimum isotropic force of 12 N when a maximum motor torque of 4 Nm is used. A value of 12 N for the isotropic force seems enough for a guidance including gravity compensation of the robot links. However, this had to be confirmed experimentally in further work with the real prototype. When the isotropic forces at the end effector are not sufficient, we can choose motors with higher torques or simply add a mechanical system to compensate the weight of the links like using tension spring or counterweight and thereby release the extra torque used by the motors. Since the aim of the proposed co-bot is to guide the surgeon with a force feedback, future work will consist in designing the electronic devices architecture and to propose a control system for the co-bot. Finally, we plan to evaluate, using the prototype of the co-bot, the demonstration of a brachytherapy procedure on a prostate phantom in a preclinical environment.

Acknowledgments

This work was partly supported by the French Brittany Region and by the French ANR within the Investissements d'Avenir program (Labex CAMI) under reference ANR-11-LABX-0004 (Integrated project CAPRI).

References

1. B. L. Davies, S. J. Harris and E. Dibble, "Brachytherapy" an example of a urological minimally invasive robotic procedure," *Int. J. Med. Robot. Comput. Assisted Surg.*, **1**(1), 88–96 (2004).
2. S. Marshall and S. Taneja, "Focal therapy for prostate cancer: The current status," *Prostate Int.* **3**(2), 35–41 (2015).
3. S. Tran, R. Boissier, J. Perrin, G. Karsenty and E. Lechevallier, "Review of the different treatments and management for prostate cancer and fertility," *Urology* **86**(5), 936–941 (2015).
4. H. F. Hope-Stone, S. C. Klevenhagen, B. S. Mantell, W. Y. Morgan and S. A. Scholnick, "Use of the curietron at The London Hospital," *Clin. Radiol.* **32**(1), 17–23 (1981).
5. D. Elliott, J. Berkey and G. Hoedeman, "Automated implantation system for radioisotopeseeds," U.S. patent 6869390 B2, 22 March 2005.
6. C. M. Schneider, A. M. Okamura and G. Fichtinger, "A Robotic System for Transrectal Needle Insertion into the Prostate with Integrated Ultrasound," *2004 IEEE International Conference on Robotics and Automation, 2004. Proceedings. ICRA'04*, vol. 1 (IEEE, 2004) pp. 365–370.
7. G. Fichtinger, J. P. Fiene, C. W. Kennedy, G. Kronreif, I. Iordachita, D. Y. Song, E. C. Burdette and P. Kazanzides, "Robotic assistance for ultrasound-guided prostate brachytherapy," *Med. Image Anal.* **12**(5), 535–545 (2008).
8. Z. Wei, M. Ding, D. Downey and A. Fenster, "3D TRUS Guided Robot Assisted Prostate Brachytherapy," *International Conference on Medical Image Computing and Computer-Assisted Intervention* (Springer, Berlin, Heidelberg, 2005) pp. 17–24.
9. S. Okazawa, R. Ebrahimi, J. Chuang, S. E. Salcudean and R. Rohling, "Hand-held steerable needle device," *IEEE/ASME Trans. Mechatron.* **10**(3), 285–296 (2005).
10. L. Phee, D. Xiao, J. Yuen, C. F. Chan, H. Ho, C. H. Thng, C. Cheng and W. S. Ng, "Ultrasound Guided Robotic System for Transperineal Biopsy of the Prostate," *Proceedings of the 2005 IEEE International Conference on Robotics and Automation, 2005. ICRA 2005* (IEEE, 2005) pp. 1315–1320.
11. M. Meltsner, N. Ferrier and B. Thomadsen, "SU-FF-T-03: Design and quantitative analysis of a novel brachytherapy robot," *Med. Phys.* **32**(6Part6), 1949–1949 (2005).

12. H. Bassan, T. Hayes, R. V. Patel and M. Moallem, "A Novel Manipulator for 3D Ultrasound Guided Percutaneous Needle Insertion," *2007 IEEE International Conference on Robotics and Automation* (IEEE, 2007) pp. 617–622.
13. S. E. Salcudean, T. D. Prananta, W. J. Morris and I. Spadinger, "A Robotic Needle Guide for Prostate Brachytherapy," *IEEE International Conference on Robotics and Automation, 2008. ICRA 2008* (IEEE, 2008) pp. 2975–2981.
14. N. Hungr, J. Troccaz, N. Zemiti and N. Tripodi, "Design of An Ultrasound-Guided Robotic Brachytherapy Needle-Insertion System," *Annual International Conference of the IEEE Engineering in Medicine and Biology Society, 2009. EMBC 2009* (IEEE, 2009) pp. 250–253.
15. S. Jiang, J. Guo, S. Liu, J. Liu and J. Yang, "Kinematic analysis of a 5-DOF hybrid-driven MR compatible robot for minimally invasive prostatic interventions," *Robotica* **30**(7), 1147–1156 (2012).
16. N. Plitea, A. Szilaghyi and D. Pisla, "Kinematic analysis of a new 5-DOF modular parallel robot for brachytherapy," *Robot. Comput. Integr. Manufact.* **31**, 70–80 (2015).
17. http://www.cnrs.fr/lettre-innovation/actus.php?numero=341.
18. T. K. Podder, L. Beaulieu, B. Caldwell, R. A. Cormack, J. B. Crass, A. P. Dicker, A. Fenster, G. Fichtinger, M. A. Meltsner, M. A. Moerland, R. Nath, M. J. Rivard, T. Salcudean, D. Y. Song, B. R. Thomadsen and Y. Yu, "AAPM and GEC-ESTRO guidelines for image-guided robotic brachytherapy: Report of Task Group 192," *Med. Phys.* **41**(10), 101501 (2014).
19. B. Al-Qaisieh, J. Mason, P. Bownes, A. Henry, L. Dickinson, H. U. Ahmed, M. Emberton and S. Langley, "Dosimetry modeling for focal low-dose-rate prostate brachytherapy," *Int. J. Radiat. Oncol. Biol. Phys.* **92**(4), 787–793 (2015).
20. A. Riwan, B. Giudicelli, F. Taha, J.-Y. Lazennec, A. Sabhani, P. Kilian, Z. Jabbour, J. VanRhijn, F. Louveau, G. Morel, V. Francoise, D. Armand and S. Lavallee, "Surgico-bot project: Robotic assistant for spine surgery," *Innovat. Res. BioMed. Eng.* **32**(2), 130–134 (2011).
21. C. Poquet, P. Mozer, G. Morel and M.-A. Vitrani, "A Novel Comanipulation Device for Assisting Needle Placement in Ultrasound Guided Prostate Biopsies," *IEEE IROS*, 4084–4091 (2013).
22. R. L'Orsa, C. J. Macnab and M. Tavakoli, "Introduction to haptics for neurosurgeons," *Neurosurgery* **72**(1), 139–153 (2013).
23. R. Clavel, Conception d'un robot paralle rapide 4 degrés de libertés *Ph.D. Thesis* (EPFL, Lausanne, Switzerland, 1991).
24. M. Opl, M. Holub, J. Pavl, F. Brad, P. Blecha, J. Kozubk and J. Coufal, "DELTA - Robot with Parallel Kinematics," *Proceedings in Mechatronics* (Springer, 2011) pp. 445–452.
25. C. Gosselin and J. Angeles, "Singularity analysis of closed-loop kinematic chains," *IEEE Trans. Robot. Autom.* **6**(3), 281–290 (1990).
26. Y. Yu, T. K. Podder, Y. D. Zhang, W. S. Ng, V. Misic, J. Sherman, D. Fuller, D. J. Rubens, J. G. Strang, R. A. Brasacchio and E. M. Messing, "Robotic system for prostate brachytherapy," *Comput. Aided Surg.* **12**(6), 366–370 (2007).
27. www.onshape.com.
28. G. Fichtinger, T. L. DeWeese, A. Patriciu, A. Tanacs, D. Mazilu, J. H. Anderson, K. Masamune, R. H. Taylor and D. Stoianovici, "System for robotically assisted prostate biopsy and therapy with intraoperative CT guidance," *Acad. Radiol.* **9**(1), 60–74 (2002).
29. D. Karnopp, "Computer simulation of stick-slip friction in mechanical dynamic Systems," *J. Dyn. Syst. Measure. Controls*, **107**(1), 100–103 (1985).
30. O. Egeland and J. T. Gravdahl, "Modeling and Simulation for Automatic Control," **In:** *Marine Cybernetics AS* (2002). Trondheim, Norway
31. http://graphics.cs.msu.ru/en/node/909.

https://doi.org/10.1017/S026357472000051X Published online by Cambridge University Press